Systematic Testing of Improved Designs of Miniaturized LaB_6 Hollow Cathodes for Electric Propulsion Systems for CubeSats and Small Satellites

IEPC-2019-428

Presented at the 36th International Electric Propulsion Conference, University of Vienna, Austria September 15-20, 2019

George-Cristian Potrivitu[1], Luxiang Xu[2] and Shuyan Xu[3]
Plasma Sources and Application Centre/Space Propulsion Centre, NIE, Nanyang Technological University, Singapore 637616

Abstract: Self-sustained operation at low-current emission (< 1 A) and low-power start-up are prime requirements for hollow cathodes employed with miniaturized space solar electric propulsion systems. Two LaB_6 hollow cathode designs were developed and systematically tested at PSAC/SPCS in the attempt of producing suitable devices for low-power electric propulsion thrusters. Material selection, cathode geometry and thermal management were the main driving factors in improving the cathodes performance and lower their power consumption. Moreover, a novel, proof-of-concept orifice-less cathode design included a knife-edge LaB_6 emitter for enhanced electric field during cathode start-up and steady-state operation and was exhaustively tested. The cathodes were tested with Xenon in diode and triode configuration with an external anode and keeper electrode as well as in conjunction with a low-power Hall thruster. Discharge mode transitions were recorded over a wide range of anode current, keeper current and mass flow rate. Thermal measurements were also conducted in order to assess for the cathode thermal management improvements and compared with computer simulations.

Nomenclature

D_o	= cathode orifice diameter
I	= discharge current
j	= current density
J_0	= equivalent mass flow rate
ID	= inner diameter
OD	= outer diameter
PSAC	= Plasma Sources and Applications Centre
SPCS	= Space Propulsion Centre Singapore
TC	= thermocouple
V	= potential/voltage
W	= atomic mass number
ΔV	= potential drop
ε	= emissivity
ε_i	= ionization potential

I.Introduction

IN recent years, the field of spacecraft propulsion systems undertook a major shift towards the solar electric propulsion. The latter saw a rocket development and it is believed to monopolize the market, or at least several specific market sectors, in the near future. Such systems proved to be capable of working with a very high system fault tolerance for long durations, up to years, offering a reduction in the need of propellant, translated into higher payloads or lower costs to access the space. Their high versatility and robustness, proved during several interplanetary missions, recommend them for Earth orbit missions. The space industry trends show that there is a higher interest in small satellites for low Earth orbit (LEO) missions[3,4]. On average, the mass

[1] PhD Candidate, PSAC/SPCS, nie17potr7281@e.ntu.edu.sg
[2] Research Engineer, PSAC/SPCS, luxiang.xu@nie.edu.sg
[3] Professor, PSAC/SPCS, shuyan@ntu.edu.sg

of the satellites placed on LEO decreased with 33% from 2000 to 2016[1], while for the geostationary orbit (GEO) missions the average spacecraft mass increased with 50% in the same time span[1]. There is a continuous tendency towards the deployment of massive LEO satellite constellations with hundreds of small spacecrafts[4]. Therefore, the interest for robust, efficient and reliable propulsion system is an imperative in the current space sector paradigm.

Although the high-power electric propulsion drives are ideal for GEO missions and interplanetary travel, for low orbit missions and for light platforms (nano-, micro- and mini-satellites; 10-500 kg[2]) low-power systems should be developed. Such systems should be capable to be onboarded on small satellites (a few U satellites; 1 U = 10 cm x 10 cm x 10 cm), to deliver thrust up to several tens of mN and relatively high cumulative delta-V. Therefore, highly efficient electric propulsion drives are to be designed, tested and optimized in order to match the market tendency towards small but autonomous platforms, thus with propulsive systems[3-5]. Moreover, due to the increasing number of debris on low orbits it would be necessary that each satellite is equipped with a thruster capable to undergo a controlled deorbiting at the end of mission. Ideal candidates for attitude determination and control systems (ADCS) are the field-emission electric propulsion (FEEP) systems, the vacuum arc thrusters (VAT) or the arcjets. However, in the range of 45 W to 100 W the Hall thruster technology can be the perfect candidate for the job, producing relatively high thrust with a high efficiency, allowing them to be used as main propulsive system and as ADCS, thus offering both off-orbit and in-orbit autonomy.

The classical design of the Hall thrusters should be optimized in order to produce highly efficient thrust at low input voltages. In the latter years several solutions have been found, among which the wall-less thrusters[30-33] and the magnetically shielded thrusters[34-38] have proved to withstand the pressure of the experimental campaigns, showing promising results. A crucial component of a Hall thruster wall-less or magnetically shielded, remains the cathode. As the power level is drastically decreased, the discharge current during operation is usually under 1 A. The electron current necessary for the discharge sustenance and for plume neutralization is produced by the cathode, thus low-current cathode technology is an important point on the agenda. Hollow cathodes capable to operate in self-sustained mode should be designed and optimized to operate together with the low-power thrusters, having low power consumption just during the ignition phase. Sub-100 W Hall thrusters require hollow cathodes capable to operate in a self-sustained mode at current levels < 1 A, while the start-up power should not exceed 50 W. This paper presents the results of recent research on low-current hollow cathodes designed to match the above-mentioned requirements and development at PSAC/SPC Singapore. Two low-current, orifice-less LaB_6 hollow cathodes were developed and systematically tested, featuring emitters with knife-edges. The two cathodes, based on the PSAC cathode design[11], have improved thermal behavior and were tested with Xe in standalone mode (diode and triode configuration with an external anode and keeper electrode) and in conjunction with a Hall thruster. The paper presents the results for the cathodes discharge characterization, from ignition tests to operation in standalone mode and with a Hall thruster as well as thermal characterization.

II.Low-current hollow cathode design

The focus of the current research is to produce hollow cathodes that can ignite at lower heating power levels. The target heating power for start-up is below 50 W to match the power capabilities of small satellites. Once ignited, the cathode should be able to operate in self-sustained mode with no requirements for heating or keeper power. Moreover, it is important that the cathode discharge is stable, namely in a spot mode[9,19,39-42].

Cathode #1 Cathode #2

Figure 1. Low-current hollow cathode #1 and cathode #2 after experiments.

The design of new hollow cathodes is based on the understanding of the physics that governs the operations of such devices. A baseline cathode serves as the starting point, providing the main geometrical features, material selection[6] and, most importantly, manufacturing, assembly and integration know-how. An innovative idea can open the path to models that overcome some of the existing drawbacks of such devices (heating power level, stable operation at low emission current, reduced lifetime and ignition robustness). For instance, the designs presented in this paper are based on an innovative geometry of the cylindrical hollow emitter which presents a 45° knife-edge at one of its ends. Such a geometrical feature comes with its challenges in terms of machining but can highly modify the power balance needed for the cathode start-up and operation. Because the thermal aspect of the cathode remains highly important, the path to the development of new models has the thermal modelling at its center, underpinned by iterative thermal simulations to meet the requirements. This process is bolstered by geometry changes and material selection. Once the thermal modelling converges, the designs are refined via further modelling including electrostatic, propellant flow and plasma simulations.

Two new low-current LaB_6 hollow cathodes were designed departing from the baseline cathode design, PSAC cathode[11], and incorporating an emitter with the shape of a hollow cylinder with a knife-edge and a better thermal management based on additional thermal shielding. The cathodes, fully assembled, are shown in Fig. 1. The knife-edge geometry of the emitter was chosen in the attempt of producing and sustaining a stronger electric field at the emitter exit region, which in turn may facilitate the cathode initial discharge and reduce the required heating power. Moreover, a stronger electric field during steady-state operation can be beneficial, while an orifice-less geometry may allow for a deeper plasma penetration in the emitter region[7]. Cathode #1 has a rather conservative design, closer to PSAC cathode, but incorporates the knife-edge emitter. Cathode #2 has reduced dimensions, smaller keeper orifice diameter, knife-edge emitter and an additional thermal shield placed within the keeper insulator. The emitters have the same emission surface area as PSAC cathode, 0.76 cm^2. The cathodes' design was refined through iterative thermal simulations based on geometry alterations and material selection as well as electrostatic and propellant flow simulations.

III. Experimental setup

The new cathodes were firstly tested in standalone configuration together with an external anode in the Cathode Experiments Vacuum Chamber (CEVAC)[11]. Once the cathode discharge envelopes and thermal management tests were concluded, the cathodes were further tested together with a Hall thruster to verify their ability in providing enough emission current for the stable operation of a Hall thruster. The later tests were conducted in the Thruster Experiments Vacuum Chamber (TEVAC). Hereinafter, a short description of the two vacuum testing facilities is presented.

The CEVAC at PSAC/SPCS is a vacuum chamber made of stainless steel and has a diameter of 0.4 m with a capacity of 40 l. The pressure inside the chamber can reach 5×10^{-6} mbar-N_2 and is attained by using a KYKY RVP6 dry rotary pump and a 600 l s^{-1} KYKY FF 160/620E turbomolecular pump to evacuate light gases. The chamber is accessed through a 0.4 m-diameter door located at the top of the chamber.

The TEVAC vessel at PSAC/SPCS is made of stainless steel and has a capacity of 275 l. The pressure inside the chamber can reach 4×10^{-6} mbar-N_2 and is attained by using a Bluffton Motor Works dry rotary pump and a 520 l s^{-1}-N_2 Pfeiffer TCP 600 turbomolecular pump to evacuate light gases. Moreover, the chamber is equipped with two cryogenic pumps, ULVAC Cryogenics Cryo-U12HLE, with a pumping speed for N_2 of 4000 l s^{-1} and typical surface temperature of 13 K. The TEVAC chamber is accessed through a $0.3 \text{ m} \times 0.6 \text{ m}$ hatch located at the top of the chamber. Both chambers are equipped with observation windows which provide view access to the interior of the chambers and several power, gas and thermocouple feedthroughs. The experiments were conducted with xenon, 99.999% purity. The gas was supplied at 1.5 bar from a pressurized tank. The gas mass flow rate was controlled with Sevenstar D07 Series mass flow controllers calibrated for xenon. Figure 2-*a)* depicts cathode #1 installed in CEVAC with the external anode and Fig. 2-*b)* depicts cathode #2 installed in TEVAC together with the Hall thruster.

Apart from the electrical measurements that are discussed later in the section, the chambers were equipped with several K-type thermocouples. The thermocouples output was read and recorded using BERM Rex C-100 PID controllers. Most of the thermocouples were rated for temperatures up to 673.15 K, while some of them were rated for 1648.15 K. By using this last type of thermocouples, the internal temperature in the emitter and thermal shield regions were recorded.

Anode-cathode discharge current, referred as the anode current, I_a, (standalone tests) or the discharge current, I_d, (thruster tests) was measured using a Pearson wideband current monitor (output 0.025 V per A). The anode voltage and the keeper voltage were measured using voltage probes. Two types of voltage probes were employed: Tektronix P5100 (250 MHz, 2.75 pF) and Yokogawa 700988 (400 MHz, 14 pF). The probes were connected to a Yokogawa digital oscilloscope (DLM2024, 200 MHz, 2.5 GS s^{-1}). The electrical waveforms were recorded at sampling frequency of 500 kHz, assuring a cut-off frequency of 250 kHz. This frequency is high enough to catch the usual oscillating phenomena that the anode current and voltage may exhibit in the plume of a low-current cathode[9,10]. Moreover, the thruster anode supply was connected to the thruster anode via a 20 Ω shunt resistor to ensure an easier start-up of the thruster.

a) *b)*

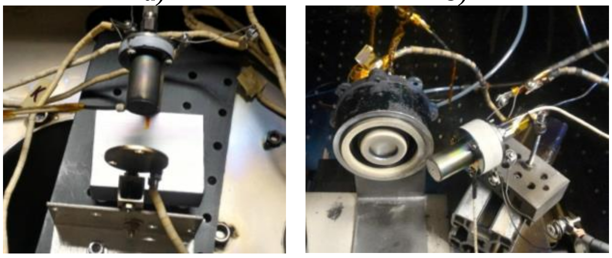

Figure 2. *a)* Cathode #1 experimental setup inside the CEVAC and *b)* experimental setup of the Hall thruster and cathode #2 in the TEVAC.

The cathodes were tested in diode and triode configuration with an external anode (charge collector). The anode used in this study was a stainless steel disc with a surface area of 5.6 cm^2 placed at 25 mm downstream of the cathode exit plate. Furthermore, one of the priorities of the current research was to test the new cathode designs in conjunction with a Hall thruster. The main duty of a hollow cathode is to provide enough emission current for the thruster discharge maintenance and plume neutralization in a stable manner. In order to test if the new designs are cable of this job, a Hall thruster was used in the TEVAC. The Hall thruster used in this study has a classical geometry with a ceramic acceleration channel and employed electromagnetic coils for magnetic field generation. The thruster's magnetic coils require less than 1 W of power, on average, and the internal and external coil are electrically connected in parallel. The thruster can stably operate at discharge potentials from 110 to 270 V with Xe mass flow rates ranging from 0.3 to 0.7 mg s^{-1}. This thruster was previously used in one of our recent studies[14]. When tested with the Hall thruster, the cathodes were placed 10 mm from the thruster's channel outer ceramic ring and inclined 45° with respect to the thruster centerline, as shown in Fig. 2-*b)*.

IV.Cathode discharge characterization

There are two main ways of testing hollow cathodes:

1. In standalone mode with and external anode (metal plate or cylinder)-this is known as diode configuration or triode configuration if the keeper electrode is also used;
2. In conjunction with a Hall thruster.

During the start-up tests the new devices are expected to produce their first plasmas. Such tests provide the start-up characteristics in terms of heating power, keeper potential and imposed current, anode potential and imposed emission current and the cathode mass flow rate. Once the cathode is in steady-state stable operation, the discharge envelopes can be constructed in order to test the stability range of the device by varying the mass flow rate, anode current and keeper current. Standalone (diode or triode) and thruster discharge envelopes can be constructed for cathode models with different geometries (keeper orifice aspect ratio, emitter dimensions etc.).

In order to construct the cathodes' operating envelopes, *i.e.* discharge characteristics, the cathodes were operated with Xe in diode configuration with the external anode and in triode configuration with both the external anode and the keeper. Moreover, in order to test the cathodes ability to function together with a thruster and fulfilling their main purpose, the two cathodes were tested in conjunction with a Hall thruster.

For the standalone testing in diode and triode configuration with an external anode and keeper electrode, data was gathered for four Xe mass flow rates: 0.057 mg s^{-1}, 0.096 mg s^{-1}, 0.14 mg s^{-1} and 0.21 mg s^{-1}. The anode current was varied from 0.1 A to 1.0 A with an increment of 0.1 A. The keeper current was set at 0.05 A, 0.10 A and 0.15 A. When stable, the cathodes were operated with no keeper current, in diode configuration with the external anode.

It is worth stating that most the measurements (except for the ones with the cathodes in self-sustained mode and in conjunction with the thruster) were conducted with the cathodes continuously receiving a heating power of approximately 34 W. Between each change in the mass flow rate or anode/keeper current, the cathodes were allowed to operate for 300 s before any current/voltage probe measurements were recorded. This was to ensure a stable operation of the cathodes at each new operating condition, imposed by the cathodes reaching their thermal equilibrium. In the following sections the cathodes ignition characteristics and operating envelopes are presented. Cathodes discharge mode maps are constructed based on the spot/plume transition criterion. Self-sustained operation results are also presented as well as the results from thruster operation. The cathode operating mode (spot/plume) and mode transition was assessed based on the time waveforms of the anode current and by employing the mode criterion: spot mode corresponds to the ratio of the anode current's standard deviation to anode current's mean value, $I_{a,std}/I_{a,mean}$, being under 9%, while plume mode correspond to ratios over 9%[7-10].

A. Cathode ignition characteristics

In order to initiate the cathodes discharge, the heating power was gradually increased over 10 min to approximately 43 W for cathode #1 and 35 W for cathode #2. Cathode #1 was started with an average Xe mass flow rate of 0.15 mg s^{-1}, while for cathode #2 the mass flow rate was set to 0.21 mg s^{-1}, for standalone mode, and 0.1 mg s^{-1}, when operating with the thruster. The secondary discharge was established by imposing a keeper voltage, V_k, between 150 V to 900 V, with a keeper current, I_k, limited to 0.10 A. Once the secondary discharge was established, the primary discharge was enabled by biasing the external anode at a potential, V_a, of 200-250 V and limiting the anode current, I_a, to 0.10 A. All the measurements were conducted with the anode and keeper power supplies operating in a "current regulated" manner. The start-up sequence includes the cathode heating and the ignition of the keeper discharge. With the keeper discharge ignited, it was always possible to establish the anode discharge.

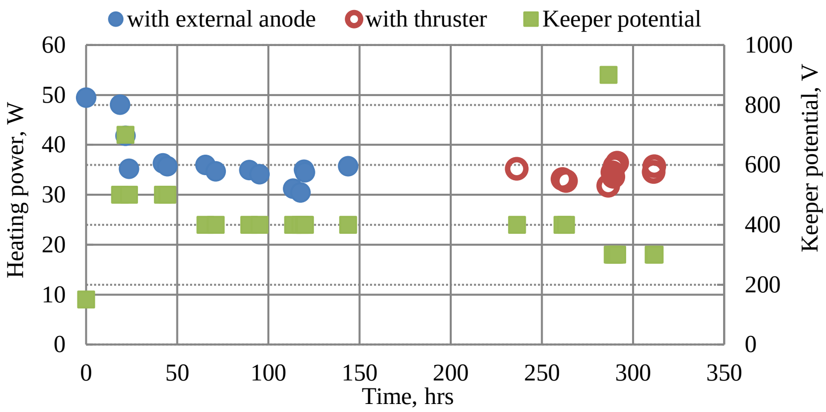

Figure 3. Cathode #2 heating power and keeper potential required for start-up with the external anode and with the thruster over the experimental campaign duration.

Table 1. Summary of the cathodes operating time.

Operating hours	Cathode #1	Cathode #2
With external anode (Xe)	23.33	28.89
With external anode (Kr)	18.5	0
With Hall thruster	14.35	164.11
Ignitions	43	50
Total	56.18	193

Table 2. Summary of the cathodes start-up characteristics.

	Cathode #1	Cathode #2
Average heating power, W	43.07	34.41
Average keeper potential, V	460.8	414
Average mass flow rate, mg s^{-1}	0.15 (standalone and thruster)	0.21 (standalone) 0.1 (thruster)
Average cathode base temperature, °C	277 (standalone) 365 (thruster)	235 (standalone) 263 (thruster)

Cathode #2 proved to have the best thermal management, allowing for a much lower heating power. The results for cathode #2 are depicted in Fig. 3. The average start-up heating power was around 34.4 W, almost 10 W lower than in the case of cathode #1 and up to 34 W lower than the PSAC cathode. The initial heating power over the first couple of ignitions was high, reaching almost 50 W, a normal behavior for new cathodes. As a result, when tested in standalone mode, the average start-up heating power was 36.8 W, over 15 ignitions. During the tests, the keeper voltage ranged from 150 to 700 V with a current limited to 0.1 A, while the cathode mass flow rate was set at 0.21 mg s^{-1}. During the 10 ignitions with the thruster in the TEVAC, the average start-up heating power was 34.3 W, while the cathode mass flow rate was set at 0.1 mg s^{-1}. The keeper potential varied between 300 and 900 V, with a current limited at 0.1 A. Cathode #2 cumulated slightly over 43 hours of continuous operation during the tests. Additionally, the cathode was employed in a lifetime test for a Hall thruster, cumulating over 150 hours and 25 ignitions, leading to a total operational time of 193 hours and 55 successful ignitions. A summary of the cathodes' operating time is presented in Table 1, while Table 2 contains a summary of the cathodes' start-up characteristics.

a) *b)*

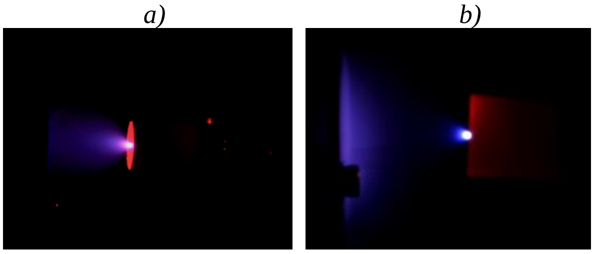

Figure 4. *a)* Cathode #1 discharge plume (1 A-anode current, 0.1 A-keeper current, 0.14 mg s^{-1}-Xe) and *b)* cathode #2 discharge plume (1 A-anode current, 0.21 mg s^{-1}-Xe). Both cathodes are operating with the external anode in the CEVAC.

B. Cathode standalone operation

The cathodes were firstly tested in standalone mode with the external anode and their operational characteristics were analyzed. Figure 4 depicts the plasma plumes of the two cathodes during standalone testing.

The discharge characteristics for cathode #1 are presented hereinafter. The cathode was firstly tested in triode configuration with the keeper electrode and the external anode and in diode configuration only with the external anode (the keeper electrode was kept floating). The cathode's anode characteristics and discharge mode map are presented in Fig. 5-*a)*. The cathode exhibited negative anode discharge impedance, $Z_a \sim 1/I_a$ for anode current values up to 0.7 A, followed by a slightly positive or constant discharge impedance thereafter. The reduction in the discharge impedance suggests a lowering in the cathode sheath potential at higher discharge current levels[12]. The anode potential ranged from 120 V to less than 45 V across the range of discharge current and keeper current imposed to the system, decreasing with the increase in the cathode mass flow rate and keeper current. It is worth mentioning that the cathode exhibited stable operation only at the xenon mass flow rates of 0.096 mg s^{-1}, 0.14 mg s^{-1} and 0.21 mg s^{-1}, no data being recorded at the mass flow rate of 0.057 mg s^{-1}.

The keeper voltage ranged between 4.5 and 88 V, following the same trends as the anode voltage: decreasing with the increase in the cathode mass flow rate and anode current. Moreover, the keeper discharge exhibited only positive impedance, the keeper voltage increasing with the keeper current. Given this fact, the cathode total power (which includes the constant heating power) remained almost constant for a specific mass flow rate, disregarding the keeper current, and increasing with the increase in the anode current. This proves that although important in stabilizing the cathode discharge, the keeper discharge does not highly impact the overall power of the system.

Spot mode operation was observed only when the total emission current was over 0.5 A (both anode and keeper) and for the mass flow rates of 0.14 mg s^{-1} and 0.21 mg s^{-1}. The anode voltage averaged 50.3 V. Spot mode operation was characterized by values of the ratio, $I_{a,std}/I_{a,mean}$, below 9%, with quiescent spectra of the anode current, as previously reported in literature[7-10]. Most of the operational points at the mass flow rate of 0.098 mg s^{-1} and anode current over 0.7 A were characterized by diffuse mode operation with very high oscillations in the discharge current and with a highly diffuse plume attached to the vacuum chamber walls, previously described in literature[13]. The cathode discharge had positive impedance proving that at this mass flow rate it was difficult to sustain emission currents over 0.7 A.

The cathode was operated in self-sustained mode, *i.e.* no heating power applied, only at the anode current of 1 A. An increase in the keeper current induced a reduction in the anode discharge impedance, as presented in Fig. 5-*b)*. However, an increase in the keeper current induced an increase in the anode current oscillations level. At the mass flow rate of 0.096 mg s^{-1}, the cathode operated in plume mode with a power levels from 65 to 70 W, decreasing with the increase in the keeper current. At the mass flow rate of 0.14 mg s^{-1}, the cathode operated in spot mode with an increase in the anode current oscillations as the keeper current was increased, but remaining below 9%, with respect to the average

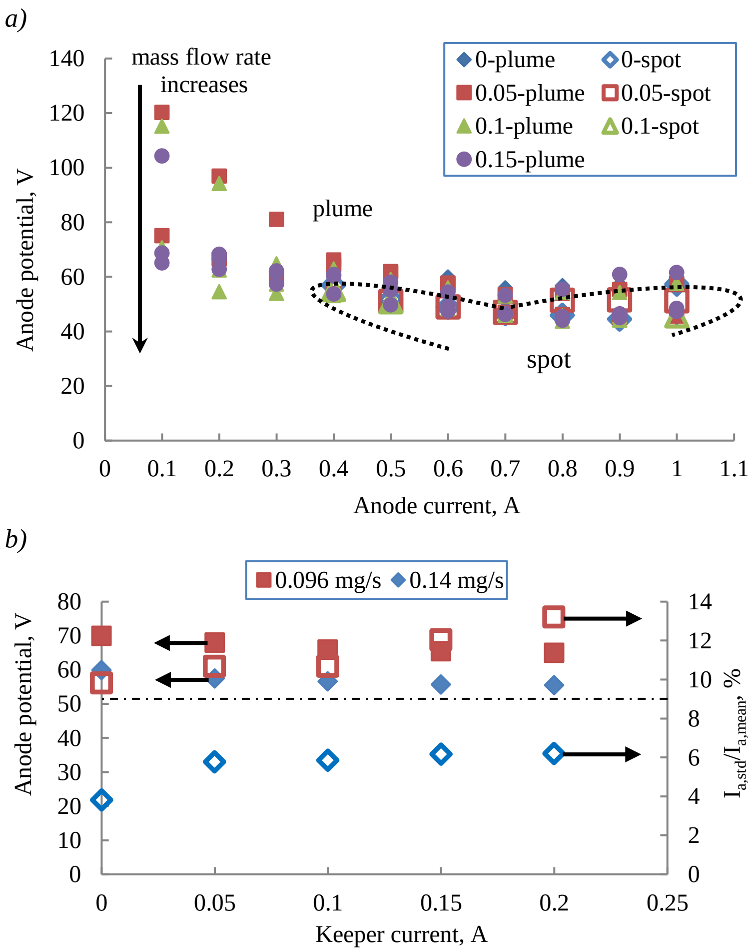

Figure 5. ***a)*** **Cathode #1 discharge mode map for the mass flow rates of 0.098 mg s^{-1}, 0.14 mg s^{-1} and 0.21 mg s^{-1} and for the keeper currents of 0 A, 0.05 A, 0.10 A, 0.15 A and *b)* cathode #1 self-sustained operation: anode potential and ratio $I_{a,std}/I_{a,mean}$ as a function of the keeper current and for different cathode mass flow rates; the anode current is 1 A and the dotted line at 9% indicates the threshold for plume/spot mode transition.**

level (3.8-6.2 %). The cathode operation power dropped to under 60 W. It is worth noticing that at the same mass flow rate and at the anode current of 1 A, the cathode showed plume mode operation when the heating power was applied, suggesting that an overheating of the cathode can induce the onset of the detrimental plume mode. At higher mass flow rates, the cathode operation became highly unstable and the discharge extinguished frequently. It is believed that the wear of the cathode (being previously employed in experiments with Kr and a Hall thruster) highly impacted its ability to maintain stable discharges beyond a very narrow range of mass flow rates.

C. Cathode operation against Hall thruster

An important aspect in a cathode development is the operation against a low-power Hall thruster. By coupling the cathode with the thruster, important information about the stability of the thruster operation can be provided. In the future, such tests should include also a characterization of the thruster performances, such as thrust level, efficiency and specific impulse.

The cathodes were tested with a low-power Hall thruster developed at PSAC/SPCS[6,14,15]. However, instead of a classical operation of the thruster in "voltage controlled" mode, the system was operated in "current controlled" mode, in order to assess for the ability of the cathode to provide the imposed discharge current, but with the drawback of lower discharge potentials (hence, lower thrust and specific impulse levels). The plume of the Hall thruster when operating in conjunction with cathode #1 and cathode #2 is depicted in Fig. 6. The results only for cathode #2 operation with the Hall thruster are presented hereinafter.

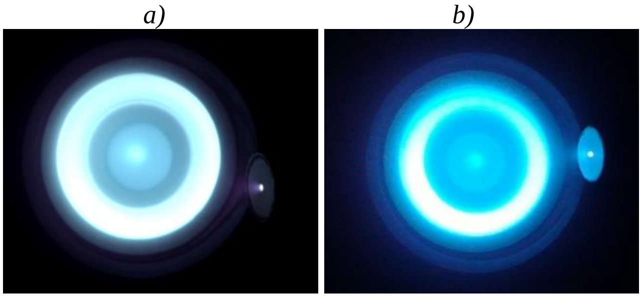

Figure 6. Hall thruster plasma plume *a)* with cathode #1 at 1 A of discharge current (the cathode mass flow rate is 0.16 mg s^{-1}-Xe and the anode mass flow rate is 0.65 mg s^{-1}-Xe with a total system power of 120 W) and *b)* with cathode #2 at 0.55 A of discharge current (the cathode mass flow rate is 0.096 mg s^{-1}-Xe and the anode mass flow rate is 0.34 mg s^{-1}-Xe with a total system power of 91.5 W).

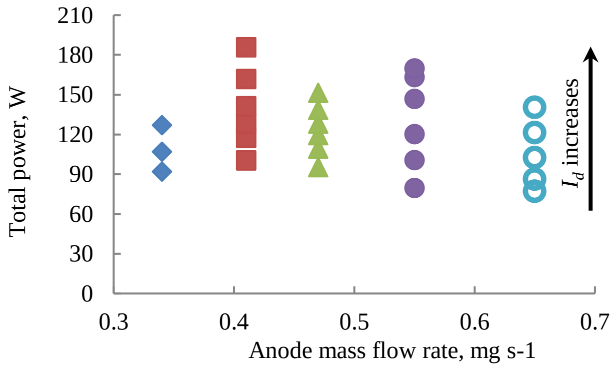

Figure 7. Hall thruster discharge power as a function of the anode mass flow rate when operating in conjunction with cathode #2, self-sustained at 0.098 mg s^{-1}-Xe. The magnet power ranged from 0.6 to 1.8 W.

The mass flow rate of the cathode was kept constant at 0.098 mg s^{-1} throughout the experiments, while the discharge current was varied between 0.5 A and 1 A for five anode mass flow rate levels from 0.34 mg s^{-1} to 0.65 mg s^{-1}. The cathode operated in self-sustained mode, with no additional keeper or heating power. The discharge voltage ranged from 120 V to 200 V, decreasing with the increase in the anode mass flow rate. The cathode showed a more stable operation at the given conditions compared to cathode #1, seen in the low level of fluctuations of the discharge current, under 5% of the average value. It was also observed that by adding a small keeper current, under 0.1 A, the discharge voltage diminished, but with little impact on the level of fluctuations in the discharge current. The system total power during the experiments is presented in Fig. 7. The thruster-cathode system consumed a power between 90 and 185 W, increasing with the increase in the discharge current and decreasing with the increase in the anode mass flow rate.

V. Thermal management characterization

The cathode heater is the main source of thermal load applied to the emitter in order to reach the required thermionic emission temperature. Both cathode #1 and cathode #2 have heaters with similar designs containing windings of a tungsten-rhenium filament. Because cathode #1's filament is longer than the one of cathode #2, due to the larger dimensions of the ceramic support part, its heater provides more power at the same heating current level. It is worth stating that cathode #1's heater characteristic is identical to the one of the PSAC cathode.

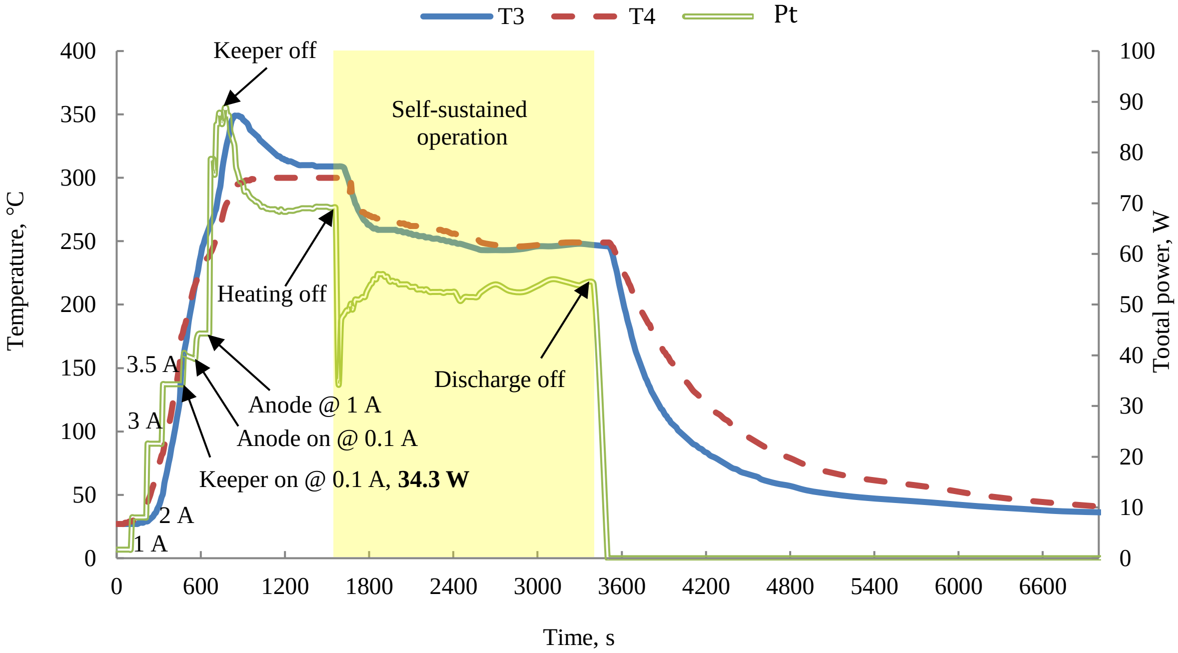

Figure 8. Time variation of the temperature recorded by the thermocouples T3 and T4 during cathode #2 heating, start-up, continuous operation and cooling-off.

The cathodes' thermal management was characterized using K-type thermocouple measurements. Two sets of tests were conducted: 1. with the heater on and no discharge, while the thermocouples were placed at various locations on the cathodes; 2. continuous temperature measurements at the keeper base and cathode base during the start-up and cathodes' steady-state operation (plasma on), those two locations being regarded as boundary conditions for the cathodes' thermal behavior and providing valuable information about how the heat is dissipated from the emitter region to the cathodes' extremities. The results for cathode #2 are presented hereinafter, since this cathode proved to have a better thermal behavior. For cathode #2 four thermocouples were placed as follows: T1 was inserted through the keeper orifice and bended, in order to touch the thermal shield Ta foils wrapped around the emitter; T2 was touching the rim of the keeper orifice plate; T3 was touching the keeper electrode base and T4 was introduced in one hole of the cathode stainless steel base until it touched the lower layer of the second thermal shield. Thermal simulations conducted in COMSOL (2D axisymmetric steady-state thermal simulation, heat transfer in solids model with surface-to-surface radiation implemented) provided results that are compared to the experimental data. For the thermocouple T1, the simulation results are 166°C on average higher than the experimental ones. T1 measured a temperature of 975°C at 61 W, at the thermal shield upper extremity. At the ignition power of around 35 W, the simulations showed an emitter temperature of about 1452 K, while the thermal shield edge temperature reached 1203 K (1073 K during measurements). This proves that the thermal shield manages to "shield" almost 250 degrees over less than 2.5 mm. This implied that at 35 W the emitter reached a temperature sufficient to emit 0.1 A, given the emission surface area of 0.76 cm^2.

The time variation of the temperatures measured by the thermocouple T3, placed at the keeper base, and thermocouple T4, located at the cathode base, touching the second thermal shield, is presented in Fig. 8. The total power (heating and discharge) time variation is also indicated accordingly. The test took place over almost 7000 s with the total power ranging from 0 to 89 W. Starting with 2 A of heating current applied to the heater filament, the recorded temperatures rapidly increased, reaching at 34.3 W (3.5 A) 154°C at T3 location and 177°C for T4. The keeper discharge was established by imposing a keeper potential of 400 V and a limited emission current of 0.1 A. The discharge stabilized at a power level of 5 W after 100 s. At this point, the anode discharge was established by biasing the anode at 250 V and current limited at 0.1 A. T3 recorded 222°C and T4 219°C. The primary discharge stabilized at a power level of around 6 W, while the keeper power dropped to 4 W over 100 s. Now, the anode current was increased to 1 A and over the next 100 s the anode discharge power fluctuated in the range 43-53 W, followed closely by the keeper power in the range 1.2-1.6 W. Over the same time interval, T3 recorded a rapid increase in temperature at a rate of 0.66°C s^{-1} up to a maximum of 330°C. T4 followed the same trend until it reached a temperature plateau at 300°C. After the keeper shutdown, T3 continued to rise to 350°C, while T4 remained constant at 300°C, despite the drop in the discharge power by almost 10 W. Under these conditions, the cathode operated for 760 s, while the discharge power level stabilized at 35 W, with T4 drop to meet T3 at the around 310°C. At this point, the cathode was forced into self-sustained operation by turning off the heating power and for the next 30.33 min the cathode operated in self-sustained mode. During the first 150 s, the anode discharge struggled to stabilize, and the cathode temperature rapidly reduced at a rate of 0.26°C s^{-1} for T3 and 0.2°C s^{-1} for T4. The cooling rate decreased, and both temperatures reached a plateau at about 250°C, while the anode discharge stabilized around 53 W during the next 1070 s. After other 600 s of stable operation with the temperatures reaching equilibrium, the discharge was turned off. The cathode underwent rapid cooling with T3 recording a cooling rate of 0.2°C s^{-1}, while T4 had a cooling rate of less than 0.1°C s^{-1} over the first 200 s. In order to reach the initial temperatures, the cathode needed almost 1 hour.

It is worth stating that for cathode #2, having a second thermal shield close to the cathode base, the temperatures recorded by T4 are lower than in the case of cathode #1, proving that a second thermal shield can reduce radiative losses from the heater to the cathode base. Moreover, cathode #2 exhibited stable self-sustained operation at the same discharge parameters for a much longer time than cathode #1, proving that the thermal management for this cathode was highly improved. This is supported by a lower required start-up power with over 10 W lower for cathode #2. Reaching higher temperatures at discharge extinction, the cooling rate of cathode #1 at T3 location, 0.4°C s^{-1}, is higher than the one for cathode #2, 0.3°C s^{-1}, at the same location and over the first 250 s, because of the influence of the radiative losses. Moreover, for cathode #2, thermocouples T3 and T4 recorded very close temperatures values during stable operation, with the heating power on or off. The smaller dimensions of the cathode keeper and the presence of the second thermal shield allow for a more uniform temperature of the outer parts, despite a thicker keeper insulator.

VI.Discussion: towards hollow cathode scaling and dimensioning laws

The experiments for cathode #1 stretched over 150 h, while for cathode #2 the tests took place over a period of 250 h. The thermal characterization and start-up tests showed that the cathodes can reach the required thermionic emission temperature for stable start-up at 0.1 A of emission current at much lower heating power levels compared to the baseline cathode: 43 W for cathode #1 and 34.4 W for cathode #2. This was achieved through a careful selection of materials and dimensional designing of the heater and the keeper electrode, followed by iterative thermal, electrostatic and propellant flow simulations. Moreover, the core of the cathodes, the emitter, had an innovative shape presenting a knife-edge, transforming the cathode in an orifice-less one. Such an emitter helps in imposing and maintaining a higher electric field at the emitter exit region, while the orifice-less configuration permits a deeper penetration of the electric field inside the emitter, which may in turn facilitate the initial keeper discharge. However, the keeper electrode was now biased at higher potentials, averaging 400 V. During the start-up, the heat loads on the emitter surface and keeper orifice are very high. For cathode #1, the heater thermal load reaches $4 \times 10^5\ \mathrm{W\,m^{-2}}$, while the keeper orifice heat load, having an aspect ratio of 0.66 reaches up to $8.5 \times 10^6\ \mathrm{W\,m^{-2}}$ at 400 V. For cathode #2, the heater thermal load is of $3 \times 10^5\ \mathrm{W\,m^{-2}}$, while the keeper orifice with the aspect ratio 0.5 withstands a heat load of $5 \times 10^7\ \mathrm{W\,m^{-2}}$. Thermal measurements also showed that the cathodes' bases still reach high temperatures, hence an important part of the heating power is lost through conduction and radiation from the emitter-heater region. A secondary thermal shield at the base of the cathode improves the situation. However, further optimization of the thermal shields, including material selection and manufacturing technique should be explored in order to increase the heating efficiency.

The cathodes underwent tens of ignitions and cumulated over 53 hours, cathode #1, and 193 hours, cathode #2, during the tests, showing little change in start-up parameters. However, it is important to highly expand such lifetime and ignition tests in order to match the real operation expectancy of Hall thrusters: more than 3000 ignitions and at least 5000 hours of operation[43]. After such extended periods, the emitters should be inspected in order to assess for any signs of degradation. It is believed that the knife-edge geometry of the emitters is prone to rapid degradation, leading in the end to an increase in the required heating power for the start-up.

Operational characterization of the cathodes produced results for both standalone and thruster operation. Discharge mode maps of the cathodes' discharge characteristics have been computed, proving that the cathodes can operate in spot mode, with low levels of fluctuations in the discharge current, for discharge current levels ranging from 0.5 A to 1 A and mass flow rates of 0.14 mg s^{-1} and 0.21 mg s^{-1}. However, such high mass flow rates required for spot mode operation are detrimental to the overall performance of the cathode when coupled with a thruster, since performance parameters such as specific impulse and overall efficiency are lowered. Because the cathodes are orifice-less, it was expected to have higher mass flow rate requirements for spot mode operation. This drawback can be circumvented by exploring sub-millimeter keeper orifice diameters. However, this raises challenges for the manufacturing of such small orifices, can increase the required start-up keeper potential and increase the thermal load in this region. It is known that the power loss at the keeper orifice, P_o, increases if the orifice diameter is reduced, according to the following expression[16]:

$$P_o = \frac{L_o I_d^2}{\eta \pi D_0^2}, \quad (1)$$

where η is the plasma resistivity in the orifice region and depends on plasma parameters such as electron density, electron temperature and collision frequencies between electrons and ions and electrons and neutrals. Therefore, the orifice aspect ratio must be optimized accordingly and its impact on the cathode discharge stability should be further investigated.

It was observed that, while the keeper characteristics and total power distribution followed the same trends for both cathodes, the main discharge characteristics, *i.e.* anode discharge showed differences from one cathode to another, especially at low mass flow rates. While cathode #1 exhibited anode characteristics with negative impedance, see Fig. 5-*a)*, cathode #2 discharge exhibits both negative and positive impedance (not showed here). The anode voltage is a function of the anode current, I_a, and the mass flow rate, $\dot{m}$, and is the sum of different voltage levels within the cathode[17]:

$$V_a(\dot{m}, I_a) = V_p + \Delta V_{ds1} + V_o + \Delta V_{ds2}, \quad (2)$$

where V_p is the plasma potential, ΔV_{ds1} is the planar double sheath potential drop at the emitter location, V_o is the ohmic voltage drop in the orifice channel and ΔV_{ds2} is the voltage drop due to the formation of a spherical double sheath at the keeper orifice location. The terms in Eq. (2) are complex functions of plasma property in the emitter, emitter-keeper and keeper orifice regions and are highly influenced by the imposed discharge current, internal pressure and cathode geometry. Furthermore, at the emitter surface, plasma-wall interactions can be described using a first-order approximation, by balancing the current and power equations as follows[12]:

$$j_i\left(\Phi_{sh} + \varepsilon_i + \frac{2k_B T_e}{e}\right) == j\left(\Phi_{wf,eff} + \frac{2k_B T_e}{e}\right) + j_{em}\left(\frac{3}{2}\frac{k_B T}{e} - \frac{2k_B T_e}{e}\right) + \varepsilon \sigma_{SB} T^4 + \kappa \frac{T - T_b}{L_c}, \quad (3)$$

where j_i is the ion current density collected at the emitter surface, Φ_{sh} is the sheath voltage at the emitter surface, ε_i is the first ionisation potential of the propellant atoms, $\Phi_{wf,eff}$ is the effective work function of the emitter material, j is the total current density, while the last two terms in the right-hand side of the equation account for radiation and conduction losses, with T denoting the emitter temperature, T_b the cathode base temperature and L_c the cathode tube length. An increase in the emitter temperature, due to an imposed higher discharge current, can be achieved by either increasing the sheath voltage or keeping the sheath voltage constant while increasing the ion current density through an increase in electron temperature and plasma density. However, a decrease in the sheath potential leads to a higher ion energy flux delivered to the emitter wall and triggers an increased thermionic emission and electron energy. In turn, the plasma density and electron temperature will naturally increase. Hence, the observed negative impedance of the anode discharges as a function of the anode current due to a decrease in the emitter sheath potential. In the case of diode or triode operational mode with an external anode, it is important to understand that operational parameters, such as the anode voltage, for an orifice-less cathode are complex functions of the plasma parameters in five different regions: emitter, emitter-keeper gap, keeper orifice, plume and anode. In the case of the orifice cathodes, the cathode orifice plasma region plays an important role in regulating all the operational parameters of the cathode. Therefore, the positive impedance characteristics observed for the cathode #2 (lower orifice aspect ratio and higher internal pressure) at low mass flow rates can be explained by higher voltage drops in the double sheath regions and a possible increase in the emitter sheath potential.

A proper power distribution model for low-current hollow cathodes should be established in order to link operational parameters to plasma property in the different regions of the cathode discharge. Such a model, combined with extensive and systematic testing of cathodes with altered geometries, can lead to a set of scaling and dimensioning laws that unite the geometrical parameters with the operational ones and plasma property.

This is important because no such systematic approach was ever attempted, although in the literature there can be identified research focused on hollow cathode scaling. Starting in the late 60's and ending with the beginning of the current decade, to which we can add some phenomenological laws for hollow cathode operation. However, none consider experimental results from operation against Hall thrusters, the main purpose of those cathodes and none explain how the properties and the laws apply when sizing the device from very low emission current, under 0.5 A to high emission current, say over 5 A.

The first tentative to establish such laws for low-current hollow cathodes dates to the late 1970's, when the work of Csiky[18] on low-current mercury hollow cathodes started in the late 1960's was continued by Kaufman[19] and Rehn and Kaufman[20]. Their work on orifice cathodes provided an empirical criterion for the collision parameter to describe spot mode operation based on the equivalent mass flow rate, J_0, in amperes, and the cathode orifice diameter for inert gases:

$$\frac{J_0 \sigma \sqrt{W}}{D_o} \geq 13.9 \times 10^{-20}\ \mathrm{A\ m^2 amu^{0.5}\ mm^{-1}} \quad (4)$$

where σ is the maximum value of the ionisation cross section of neutrals by electrons and W is the gas atomic mass number. They reported that no plume mode operation was recorded above this value, while no spot operation was recorded for values under 12×10^{-20} A $\mathrm{m}^2\mathrm{amu}^{0.5}$ mm^{-1}. The tests were conducted with argon, krypton and xenon. In their study, the cathodes operated at xenon equivalent mass flow rates ranging from 0.1 to 0.45 A, while the orifice diameter was varied from 0.38 mm to 0.79 mm, hence sub-millimeter orifices. In the current work, the cathodes were orifice-less with keeper orifices of 1.5 mm and 1 mm while the equivalent mass flow rates for which spot mode operation was recorded were 0.1 A and 0.15 A. Therefore, spot mode operation was recorded for collision parameter values down to 4×10^{-20} A $\mathrm{m}^2\mathrm{amu}^{0.5}$ mm^{-1}, at much lower discharge potentials and with biased keeper electrode and heating power on. However, fully self-sustained operation was recorded only for cathode #2 and at equivalent mass flow rates of 0.18 A and 0.21 A, while the collision parameter remained over 10×10^{-20} A $\mathrm{m}^2\mathrm{amu}^{0.5}$ mm^{-1}, approaching the limit described by Rehn and Kaufman. It worth investigating how the expression of the collision parameter can be changed in order to characterize cathode operation in conjunction with Hall thruster, since this study proved that the cathodes can work stably in self-sustained mode with a Hall thruster at equivalent mass flow rates as low as 70 mA.

The efforts towards hollow cathode scaling and dimensioning laws were continued by Siegfried and Wilbur[21-23] for mercury hollow cathodes and expanded by Salhi and Turchi[24-26] for high current hollow cathode operation. The model developed by Mandell and Katz[27] give a high importance to the physics of the orifice, highly influenced by the geometrical parameters of this region translated in its aspect ratio. Phenomenological models for scaling hollow cathodes were more recently developed by Capacci *et al.*[17] and Domonkos[28,29] and further expanded, using fluid modelling by Sary *et al.*[7,8].

All models fail to provide information about the difference between standalone and thruster operation of the hollow cathodes, while the aim of the further research, departing from those initial findings, is to unify such experimental results and account for both diode and triode operation with keeper electrode, external anode and low-power thrusters. Moreover, internal plasma diagnostics for orifice-less cathodes can provide instrumental insights about the operation of such devices and how the keeper orifice behaves as the main cathode orifice. Operational parameters, such as anode and keeper current and potential, can be linked to the imposed mass flow rate and the geometrical characteristics of the cathode and to the plasma parameters in the different regions of the cathode discharge. Therefore, the importance of developing suitable plasma diagnostic techniques is paramount.

Acknowledgments

This work was supported by OSTIn-SRP/EDB through the National Research Foundation, and in part by the Ministry of Education Singapore through MOE AcRF (RP6/16XS). George-Cristian Potrivitu acknowledges the support from the National Institute of Education Singapore through the NIE Ph.D. Scholarship.

References

[1]Buchen E., "SpaceWorks' 2014 Nano/Microsatellite Market Assessment", SSC14-I-3, 28th Annual AIAA/USU Conference on Small Satellites, August 2-7, Logan, UT, USA, 2014

[2]Hani K. *et. al*, *Overview of Iodine Propellant Hall Thruster Development Activities at NASA Glenn Research Center*, AIAA-2016-4729, 2016

[3]Levchenko I., Keidar M., Cantrell J., Wu Y.L., Kuninaka H., Bazaka K., and Xu S., Nature 562, 185 (2018)

[4]Levchenko I., Xu S., Mazouffre S., Keidar M., and Bazaka K, Global Challenges 2, 1800062 (2018)

[5]Levchenko I., Bazaka K., Mazouffre S., and Xu S., Nature Photonics 12, 649–657 (2018)

[6]Levchenko I., Bazaka K., Belmonte T., Keidar M., and Xu S., Adv. Mater. 30, 1802201 (2018)

[7]Sary G., "Modélisation d'une cathode creuse pour propulseur à plasma", Ph.D. Disertation, University Paul Sabatier Toulouse III, France, September 2016

[8]Sary G. *et al.*, "Hollow cathode modelling: a first approach on scaling laws", IEPC-2015-14/ISTS-2015-b-90616, Joint Conference of 30th International Symposium on Space Technology and Science and 34th International Electric Propulsion Conference and 6th Nano-satellite Symposium, Hyogo-Kobe, Japan, July 4-10, 2015

[9] Potrivitu G.C., Joussot R. and Mazouffre S., Vacuum 151 (2018), 122-132

[10]Joussot R., Grimaud L. and Mazouffre S., Vacuum 146 (2017) 52-62

[11]Potrivitu G.C. et al., "Mode Transition in a Low-current LaB_6 Hollow Cathode for Electric Propulsion Systems for Small Satellites", IEPC-2019-427, 36th International Electric Propulsion Conference, University of Vienna, Austria, September 15-20, 2019 (to be published)

[12]Albertoni R. *et al.*, "Preliminary Characterization of a LaB6 Hollow Cathode for Low-Power Hall Effect Thrusters", IEPC-2013-137, 33rd International Electric Propulsion Conference, The George Washington University, October 6-10, Washington, D.C., USA, 2013

[13]Sakai S. *et al.*, "Discharge modes and characteristics of hollow Cathode", IEPC-2007-215, 30th International Electric Propulsion Conference, Florence, Italy, September 2007

[14]Lim J.W.M. *et al.*, Plasma Sources Sci. Technol. 28, 6 (2019)

[15]Lim J.W.M. *et al.*, Journal of Visualized Experiments 144, e58466 (2019)

[16]Courtney D., “Development and Characterization of a Diverging Cusped Field Thruster and a Lanthanum Hexaboride Hollow Cathode”, Master thesis, MIT, 2008

[17]Capacci M. *et al., “Simple Numerical Model Describing Discharge Parameters in Orificed Hollow Cathode Devices”,* AIAA-97-2791, 33rd AIAA/ASME/SAE/ASEE Joint Propulsion Conference and Exhibit, Seattle, WA, 1997

[18]Csiky G. A., “Measurements of some properties of a discharge from a hollow cathode”, NASA Technical Node, NASA TN D-4966, February 1969

[19]Kaufman H.R., “Technology of Electron-bombardment Ion Thrusters”, Vol. 36, Advances in Electronics and Electron Physics, Academic Press, New-York, 1974, pp. 265-373

[20]Rehn L. and Kaufman H.R., “Correlation of Inert Gas Hollow Cathode Performance”, AIAA 78-707, 13th International Electric Propulsion Conference, San Diego, CA, April 1978

[21]Siegfried D. E. and Wilbur P. J., “A Model for Mercury Orificed Hollow Cathodes: Theory and Experiment”, AIAA-82-1889, AIAA/JSASS/DGLR 16th International Electric Propulsion Conference, New Orleans, LA, 1982

[22]Siegfried D. E. and Wilbur P. J., “A Phenomenological Model Describing Orificed Hollow Cathode Operation”, AIAA 81-0746, April 1981

[23]Siegfried D. E. and Wilbur P. J., AIAA Journal 22, 10, 1405-1412, 1984

[24]Salhi A. and Turchi P. J., “Scaling Relations for Design and Operation of Orificed Hollow Cathodes”, AIAA No. 94-3133, 30th AIAA Joint Propulsion Conference, Indianapolis, IN, June 27-29, 1994

[25]Salhi A. and Turchi P. J., “Theoretical Modeling of Orificed, Hollow Cathode Discharges”, Proceedings of the 23rd International Electric Propulsion Conference, Vol. 1, pp. 253-260, 1993

[26]Salhi A., “Theoretical and Experimental Studies of Orificed, Hollow Cathode Operation”, Ph.D. Dissertation, 1993

[27]Mandell M. J., and Katz I., “Theory of Hollow Cathode Operation in Spot and Plume Modes”, AIAA-94-3134, 30th AIAA/ASME/SAE/ASEE Joint Propulsion Conference, Indianapolis, IN, June 1994

[28]Domonkos M. T., “Evaluation of Low-Current Orificed Hollow Cathodes”, Ph.D. Dissertation, The University of Michigan, 1999

[29]Domonkos M. T., “A Particle and Energy Balance Model of the Orificed Hollow Cathode”, 38th AIAA/ASME/SAE/ASEE Joint Propulsion Conference & Exhibit, Joint Propulsion Conferences: American Institute of Aeronautics and Astronautics, 2002

[30]Tsikata S. and Mazouffre S., “Development and characterization of a wall-less Hall thruster”, EPIC Workshop, Brussels, November 2014

[31]Vaudolon J., “Electric field optimization and magnetic topology optimization in Hall thrusters”, Ph.D. Disertation, University of Orleans, France, October 2015

[32]Karadag, B. et al., “Numerical Investigation of an External Discharge Hall Thruster Design Utilizing Plasma-lens Magnetic Field”, Space Transportation Symposium ISAS/JAXA, 2015

[33]Karadag, B. et al., “Preliminary Investigation of an External Discharge Plasma Thruster”, 52nd AIAA/SAE/ASEE Joint Propulsion Conference, AIAA, Salt Lake City, UT, July 2016

[34]Mikellides, I. G. et al., Physics of Plasmas 18, 3 (2011)

[35]Hofer, R., Goebel, D., Mikellides, I., and Katz, I., “Design of a Laboratory Hall Thruster with Magnetically Shielded Channel Walls, Phase II: Experiments”, 48th AIAA/ASME/SAE/ASEE Joint Propulsion Conference & Exhibit, AIAA, Atlanta, Georgia, July 2012

[36]Conversano, R. W., Goebel, D. M., Hofer, R. R., Matlock, T. S., and Wirz, R. E., IEEE Transactions on Plasma Science 43, 1 (2015)

[37]Mazouffre, S., Vaudolon, J., Largeau, G., Henaux, C., Rossi, A., and Harribey, D., IEEE Transactions on Plasma Science 42, 10 (2014)

[38]Grimaud, L. and Mazouffre, S., Plasma Sources Sci. and Technol.26, 5 (2017)

[39]Nishiyama K., Shimizu Y., Funaki I., Kuninaka H. and Toki K., J. Propul. Power 23 (2007) 513-521

[40]Mikellides I.G., Katz I., Goebel D.M., and Jameson K.K., J. Appl. Phys. 101 (2007) 063301

[41]Jorns B.A., Mikellides I.G. and Goebel D.M., Phys. Rev. 90 (2014) 063106

[42]Jorns B.A., Dodson C., Goebel D.M., and Wirz R., Phys. Rev. 96 (2017) 023208

[43]Lev D.R., Mikellides I.G., Pedrini D., Goebel D.M., Jorns B., and McDonald M., Rev. Mod. Plasma Phys. 3, 6 (2019)